Concentrated Dispersions of Equilibrium Protein Nanoclusters That Reversibly Dissociate into Active Monomers

Keith P. Johnston,[†,‡,*] Jennifer A. Maynard,[†,§] Thomas M. Truskett,[†,⊥] Ameya U. Borwankar,[†,‡] Maria A. Miller,[†,‡] Brian K. Wilson,[†,‡] Aileen K. Dinin,[†,‡] Tarik A. Khan,[†,‡] and Kevin J. Kaczorowski[†]

[†]Department of Chemical Engineering, [‡]Center for Nano and Molecular Science, [§]Institute for Cellular and Molecular Biology, and [⊥]Institute for Theoretical Chemistry, The University of Texas at Austin, 1 University Station C0400, Austin, Texas 78712-0231, United States

ABSTRACT Stabilizing proteins at high concentration is of broad interest in drug delivery, for treatment of cancer and many other diseases. Herein, we create highly concentrated antibody dispersions (up to 260 mg/mL) comprising dense equilibrium nanoclusters of protein (monoclonal antibody 1B7, polyclonal sheep immunoglobulin G, and bovine serum albumin) molecules which, upon dilution *in vitro* or administration *in vivo*, remain conformationally stable and biologically active. The extremely concentrated environment within the nanoclusters (~700 mg/mL) provides conformational stability to the protein through a novel self-crowding mechanism, as shown by computer simulation, while the primarily repulsive nanocluster interactions result in colloidally stable, transparent dispersions. The nanoclusters are formed by adding trehalose as a cosolute which strengthens the short-ranged attraction between protein molecules. The protein cluster diameter was reversibly tuned from 50 to 300 nm by balancing short-ranged attraction against long-ranged electrostatic repulsion of weakly charged protein at a pH near the isoelectric point. This behavior is described semiquantitatively with a free energy model which includes the fractal dimension of the clusters. Upon dilution of the dispersion *in vitro*, the clusters rapidly dissociated into fully active protein monomers as shown with biophysical analysis (SEC, DLS, CD, and SDS-PAGE) and sensitive biological assays. Since the concept of forming nanoclusters by tuning colloid interactions is shown to be general, it is likely applicable to a variety of biological therapeutics, mitigating the need to engineer protein stability through amino acid modification. *In vivo* subcutaneous injection into mice results in indistinguishable pharmacokinetics *versus* a standard antibody solution. Stable protein dispersions with low viscosities may potentially enable patient self-administration by subcutaneous injection of antibody therapeutics being discovered and developed.

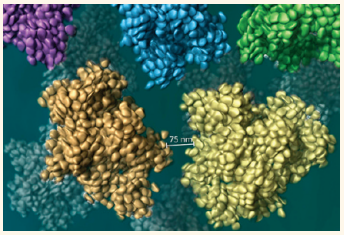

KEYWORDS: nanocluster · protein · depletion attraction · drug delivery · colloidal forces · protein stability

The crowded macromolecular environment within cells (~400 mg/mL) is known to favor the compact native state of proteins over unfolded conformations.[1,2] As described with scaled particle theory,[2,3] simulation,[4−6] and experiment,[2,7−11] not only in cells but also *in vitro*,[2,4,6−8,12,13] proteins are stabilized against unfolding by the presence of other macromolecules (volume fraction $\phi \sim 0.3$ to 0.4), which effectively "crowd out" (*i.e.*, entropically penalize) more expanded, non-native protein conformations. Simulation and theory with coarse-grain models[5,6] also predict that high concentrations ($c > 400$ mg/mL) of a single type of protein in solution favor the compact folded state *via* a mutual or self-crowding mechanism. However, stable protein solutions at these ultrahigh concentrations have not been realized experimentally since proteins are rarely soluble and tend to gel at substantially lower concentrations in part due to specific short-ranged attractive interactions, especially hydrogen bonding and hydrophobic interactions.[2,14−18] In fact, at concentrations of 100 to 300 mg/mL, proteins in solution can become increasingly susceptible to irreversible aggregation,[2,19,20] gelation and precipitation.[14,16−18] Therefore to avoid gelation, while simultaneously attaining "local" protein concentrations high enough to stabilize the native conformation *via* self-crowding, novel types of stable and reversible protein assemblies (*e.g.*, nanoclusters) are needed.

Insights into nanocluster formation and phase behavior of protein solutions may be obtained from considering model polymeric colloid suspensions.[16,17,21−25] In the latter, tunable short-range colloidal attractions (*e.g.*, cosolute-induced depletion interactions) are often present.[21,25] Strengthening such attractions (*e.g.*, by increasing cosolute concentration) causes highly polydisperse particle assemblies to form, which percolate and then gel near the colloid phase separation boundary.[21,25,26] Whereas phase separation and gelation result from strong attractions between uncharged colloids at high concentrations,[16,21,22] the physics change qualitatively when weak, longer-range electrostatic repulsion between particles is also present.[16,25] In such cases, as predicted with an equilibrium model,[27,28] long-lived and

* Address correspondence to kpj@che.utexas.edu.

Received for review October 28, 2011 and accepted January 19, 2012.

Published online January 19, 2012
10.1021/nn204166z

very large clusters of primary colloidal particles (*i.e.*, cluster/particle diameter ratio of 5−10 with low cluster-size polydispersity) have been observed in single-phase organic solvents (Figure 1a).[16,23,25,27,28] These clusters form due to the presence of short- and long-ranged interactions at the monomer scale which, in turn, produce diverse multiscale (monomer−monomer, monomer−cluster, and cluster−cluster) interactions that affect both self-assembly and transport properties of the particle dispersions.

Clusters of proteins observed to date in water have been small[23,29] ($N \sim 10$, cluster/particle diameter ratio of 2.5), dilute,[26] and short-lived.[29] Recently, reversible clusters of Au particles in water have been assembled with diameters from 30 to 100 nm (cluster/particle diameter ratios from 6 to 20) by tuning the charge on the Au particles with a weakly adsorbing nonelectrolyte.[30,31] More recently, nanoclusters have been reported for CdSe.[32] It remains a challenge to properly balance the attractive and repulsive interactions to form large clusters of proteins.

In analogy with the model colloid systems discussed above, the strength of effective protein−protein attractions in solution can also be tuned through the presence of cosolutes. For example, even cosolutes that interact weakly with the proteins still produce protein−protein depletion attraction.[3,12,33] These depletion attractions reflect the osmotic pressure imbalance that occurs when the surfaces of two protein molecules approach close enough to exclude cosolutes from the intervening gap (Figure S1 in Supporting Information). They are known to strongly influence the equilibrium behavior[2,34] and rates[2,35] of association of proteins into dimers or small oligomers. However, this behavior has received far less attention than other related crowding (*i.e.*, excluded volume) effects that low[3,9,10,12,36,37] and high[2,4,8,13] molecular weight cosolutes (crowders) have on protein folding and/or site binding. The potential of mean force for depletion attraction between proteins, $V_{dep}(r)$, is proportional to the volume fraction of the cosolute (extrinsic crowder), ϕ_E, as described with scaled particle theory[3,12] or by the Asakura−Oosawa model.[16,24,25,33,38−41] For model monomeric and oligomeric cosolutes at a fixed high concentration, V_{dep} can produce a strongly attractive osmotic second virial coefficient for a wide range in diameter ratios of extrinsic crowder to that of protein monomer from 0.02 to 1.[21,22,38,39,42] An example of a diameter ratio of 0.1 would be a 10 nm protein molecule and a 1 nm disaccharide. Thus, similar to the behavior of model colloids, depletion attractions due to small crowders—such as trehalose at high concentrations—could potentially be utilized to provide sufficient attraction to balance weak electrostatic interactions and form large protein clusters.

Herein we assemble ∼100 nm equilibrium clusters of proteins (mAb 1B7, polyclonal sheep IgG, and BSA), which dissociate into stable protein monomer upon dilution in buffer. The nanoclusters are formed simply by gently mixing lyophilized protein powder containing trehalose and buffer solution with protein concentrations up to 267 mg/mL for mAb 1B7, 350 mg/mL for IgG, and 400 mg/mL for BSA. To drive formation of large clusters in water, we (1) minimize the net protein charge with a buffer pH near the pI to weaken electrostatic repulsion, and (2) add high concentrations of a cosolute (extrinsic crowder), trehalose, to provide strong depletion attraction. The size of the clusters is either increased or decreased reversibly over a continuum by varying the concentration of cosolute (crowder), as shown by dynamic light scattering (DLS). The cluster size is predicted qualitatively by an extension of an earlier free energy model to account for the fractal dimension (δ_f) of the cluster. By adjusting ϕ_E and the pH, we balance hierarchical (protein−protein, protein−cluster, and cluster−cluster) interactions in such a way that promotes assembly of fluid dispersions of nearly monodisperse, weakly interacting protein nanoclusters with ultrahigh internal volume fractions ($\phi > 0.5$ or $c > \sim$700 mg/mL). The high internal c stabilizes proteins in their folded state *via* self-crowding, as shown theoretically.[5,6]

The stability of the protein after delivery from the clusters is of interest in protein therapeutics. After diluting the nanoclusters in buffer, the protein nanoclusters are shown to dissociate to protein monomers by dynamic light scattering (DLS),[43] size exclusion chromatography (SEC), and sodium dodecyl sulfate polyacrylamide gel electrophoresis (SDS-PAGE). The protein is demonstrated to be folded by circular dichroism (CD), thermodynamically stable by determination of the apparent melting temperature (T_m),[44] and biologically active by an enzyme-linked immunosorbent assay (ELISA).[45] Finally, the low viscosity of 40 cP, resulting from weak intercluster interactions, allows subcutaneous injection of the concentrated clusters at concentrations up to 267 mg/mL. As an indication of the ability of these dispersions to dissociate and deliver active protein, an *in vivo* bioavailability study is performed with mice. The pharmacokinetic profile of the dispersed protein nanocluster dose is compared to both subcutaneous and intravenous doses of dilute antibody solution, with activity of protein in the bloodstream quantified by both ELISA and an *in vitro* antibody neutralization assay.[46]

RESULTS AND DISCUSSION

Nanocluster Morphology and Tunability with Trehalose and Dilution in Buffer. Figure 1b shows a colloidally stable, transparent dispersion of the monoclonal antibody 1B7[45] that formed immediately upon gentle stirring of lyophilized protein powder (with a 1:1 mass ratio of trehalose to protein) in phosphate buffer solution at

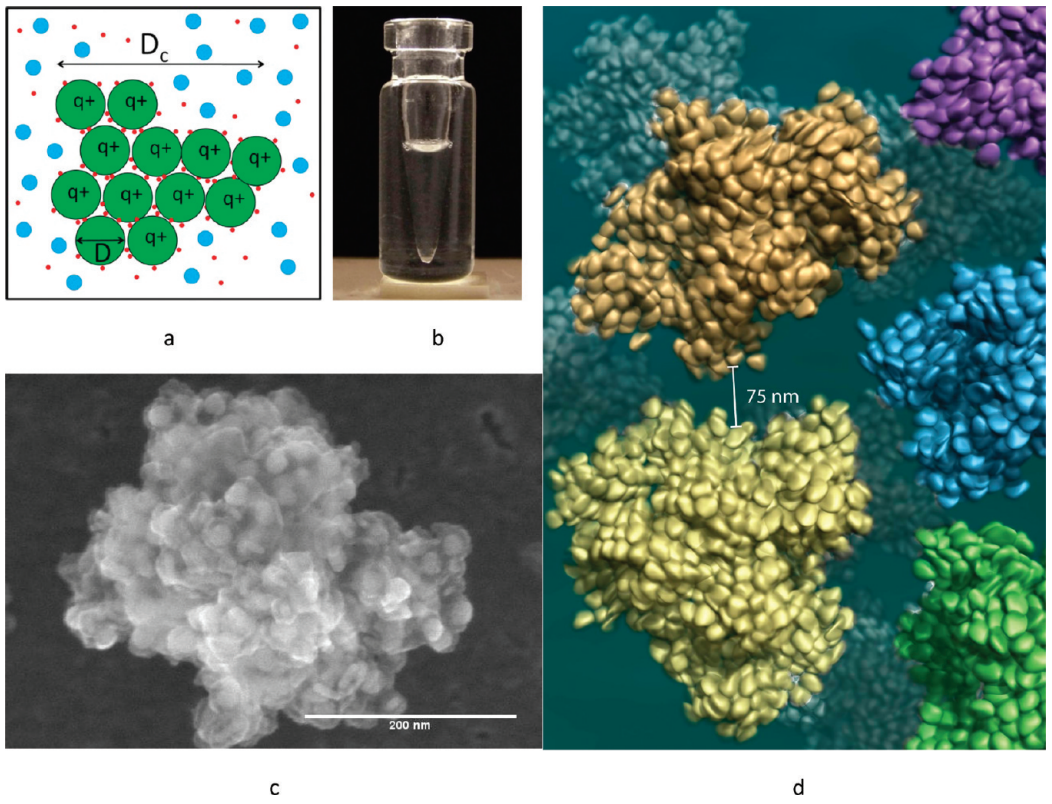

Figure 1. Nanocluster morphology for 1B7 antibody with trehalose as extrinsic crowder. (a) Schematic of protein cluster where green circles represent proteins; red dots, counterions; and blue circles, extrinsic crowders. Similar clusters are observed for colloids in organic solvent. (b) Transparent dispersion at $c = c_E = 220$ mg/mL. (c) SEM image of panel b, indicating closely spaced, self-crowded protein (the "halo" on the component particles is an artifact of trehalose deposition during sample preparation). (d) Schematic of dispersion of nanoclusters drawn to scale.

the pI (pH 7.2). The concentrations of protein, c, and extrinsic crowder, trehalose, c_E, were each 220 mg/mL. The low turbidity is a consequence of the small D_c and small difference in refractive indices of the porous cluster and solvent. The SEM images of the dispersions after cryo-preparation revealed ~300 nm nanoclusters composed of primary particles about the size of protein monomer, ~11 nm (Figure 1c and Figure S2 in Supporting Information), as shown with the help of a graphic visualizing these clusters in dispersion in Figure 1d. The "halos" about the primary particle of nanoclusters are a result of trehalose deposition during SEM sample preparation and thus of minor interest. For $c = c_E = 220$ mg/mL, the average hydrodynamic diameter, D_c, of the clusters from dynamic light scattering (DLS) was 315 nm (standard deviation in peak width of 6% over the mean) in agreement with the SEM images (Figure 2a). For the porous clusters, the volume fraction of protein within a cluster, ϕ_{int}, was measured to be 0.6 with static light scattering (SLS, Figure S3 in Supporting Information), as a function of the fractal dimension (δ_f) (eq S8 in Supporting Information). The δ_f is the slope in the log−log plot of the intensity against the scattering vector. The fractal dimension in the case of 50 nm IgG clusters was found to be 2.6 *versus* 3, 2, and 1 for completely space-filled spheres, disks, and long thin rods, respectively, which suggests that the protein has a high volume fraction inside the nanoclusters.

Upon successive dilutions of the 220 mg/mL 1B7 dispersion in phosphate buffer to maintain a constant c/c_E ratio, D_c decreased over a continuum as protein molecules left the cluster surface (Figure 2a,b). D_c then reached a plateau at ~12.3 nm for $c = c_E = 75$ mg/mL, the expected size of an antibody monomer. Similarly, dilution of c_E from 270 to 150 mg/mL with c fixed at 70 mg/mL 1B7 was used to tune the cluster size until reaching a c_E below which only ~10 nm species, presumably antibody monomers, were observed (Figure 2b,c). The trehalose concentration was decreased using pH 7.2 phosphate buffer along with small amounts of dispersion with $c = c_E = 100$ mg/mL to maintain a constant c. Upon subsequently increasing c_E back to 270 mg/mL, the original D_c values of ~300 nm were recovered. Similar experiments with a polyclonal sheep IgG mixture (Figure 2d and Figures S2b and S4 in Supporting Information) resulted in the same trends. Figure S2b in Supporting Information shows a nanocluster of sheep IgG from a dispersion at $c = c_E = 260$ mg/mL, which was diluted down to 50 mg/mL followed by cryo-preparation. The IgG nanocluster size decreased from ~80 nm at $c_E = 270$ mg/mL to ~10 nm

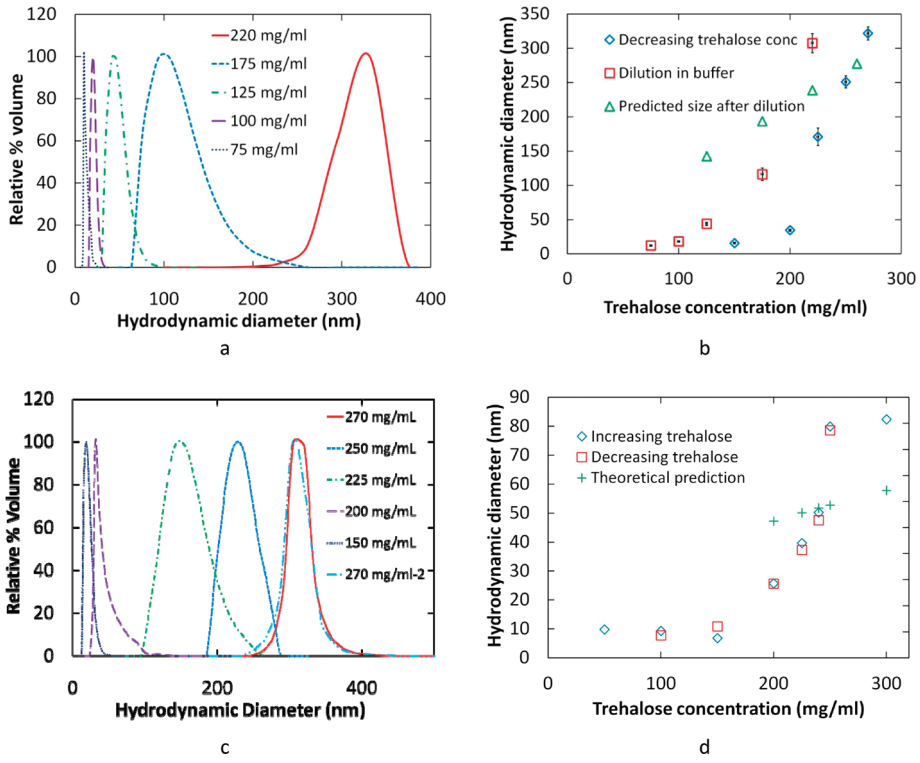

Figure 2. Hydrodynamic diameter by DLS for 1B7 antibody and polyclonal sheep IgG with trehalose as extrinsic crowder. (a) 1B7: serial dilutions in buffer such that $c/c_E = 1$. (b) 1B7: dilution in pH 7.2 phosphate buffer with starting $c = c_E = 220$ mg/mL as in panel a (squares) and decreasing c_E with a constant c of 70 mg/mL with a starting c_E of 270 mg/mL (diamonds). Error bars indicate ± SD in peak width. The predictions of eq 9 are in qualitative agreement. (c) 1B7: constant c of 70 mg/mL for decreasing c_E of trehalose from 270 to 150 mg/mL as shown in the legend and then a final point where c_E is raised back to 270 mg/mL, labeled as 270 mg/mL-2. (d) Polyclonal sheep IgG: constant c of 50 mg/mL for increasing (diamonds) followed by decreasing (squares) trehalose concentration. The reversibility suggests equilibrium cluster behavior. The theoretical predictions of eq 9 are in qualitative agreement with the data.

(monomeric protein) for $c_E = 150$ mg/mL at a constant $c = 50$ mg/mL (Figure 2d). (When increasing c_E, a 500 mg/mL trehalose solution in pH 6.4 phosphate buffer (pI of IgG) was used along with small amounts of dispersion with $c = c_E = 200$ mg/mL to maintain a constant c.) Very similar values of D_c were observed upon either increasing or decreasing the trehalose concentration. This reversibility in the nanocluster size suggests that the nanoclusters were in an equilibrium state, as further explained below with the predictions from the free energy model. The cluster size for the sheep IgG also decreases from 80 to 11 nm (monomeric protein) when the dispersion was sequentially diluted in pH 6.4 phosphate buffer from $c = c_E = 260$ mg/mL to $c = c_E = 47$ mg/mL, as shown in Figure S4 in Supporting Information. Taken together, these data demonstrate a novel type of long-lived (tested for several hours) well-defined nanocluster in aqueous media, with reversible equilibrium behavior, which was unexpected.[23,26,29]

To demonstrate further the generality of the technique, clusters were also formed with macromolecular crowders including PEG (MW 300), *N*-methylpyrrolidone (NMP), and dextran (MW 10 000). With sheep IgG at a concentration of 162 mg/mL with 162 mg/mL trehalose and 20% (v/v) PEG-300, the cluster diameter was 110 nm. For sheep IgG at a concentration of 157 mg/mL with 157 mg/mL trehalose, 10% (v/v) PEG-300 and 20% by volume NMP, the clusters were ~250 nm in diameter. Also, 315 mg/mL BSA with 5% (v/v) PEG-300 and 20% (v/v) ethanol yielded clusters of size 30 nm (BSA monomer is 4−5 nm). Whereas the focus of the current study was on a low molecular weight crowder, trehalose, these examples with macromolecular crowders, which will be the subject of a follow up report, illustrate the generality of the technique. Apart from that, in order to demonstrate the possibility of using this technique at higher concentrations of protein as a proof of concept, higher concentration dispersions of proteins were prepared. Figure 3 shows nanoclusters of BSA at a very high c of 400 mg/mL and $c_E = 240$ mg/mL which have a $D_c = 40$ nm. The number of protein monomers, about 1000, in the cluster is of the same order as the clusters formed from mAb 1B7 and sheep IgG. Highly concentrated dispersions are also shown for sheep IgG in Figure S5 in Supporting Information where nanoclusters with D_c of ~100 nm were observed for $c = 300$ and 350 mg/mL and $c/c_E = 1{:}0.5$ where trehalose was the extrinsic crowder.

Protein Stability after Dilution of the Nanoclusters. A major concern for protein formulations at high concentrations

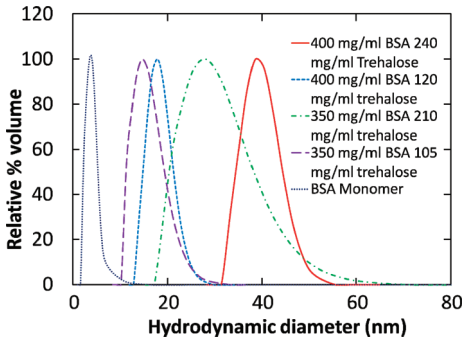

Figure 3. BSA nanocluster size for high protein concentrations. A high concentration BSA dispersion formulated at c = 400 mg/mL and c_E = 240 mg/mL forms nanoclusters with a hydrodynamic diameter of 40 nm. Dispersions formulated with lower concentrations of BSA and/or trehalose yield progressively smaller nanoclusters. Also shown is a BSA monomer which has a 4−5 nm diameter.

is the potential for individual protein monomers to misfold and form irreversible aggregates. These events may result from the dynamic nature of a protein molecule: at any given moment, a system of identical molecules will present an ensemble of related three-dimensional structures, some of which transiently expose normally buried hydrophobic patches. At low concentrations, the protein will frequently recover its native conformation, but at high concentrations,the probability of two proteins with exposed hydrophobic patches colliding and associating irreversibly is high.[9] These misfolded and irreversibly aggregated proteins do not present the native structure and therefore exhibit reduced potency and, due to their modified apparent size and exposed surface charges, altered pharmacokinetics. Moreover, the presentation of these non-native surfaces to the immune system can induce a response against the therapeutic protein, which will in itself change biological activity and pharmacokinetics.[47]

As discussed below, simulation results of earlier studies[2,5,6] suggest that the folded state is strongly favored for model proteins at high concentrations (*i.e.*, values comparable to the local protein concentration within the nanoclusters). To investigate this hypothesis, experimental studies on actual antibodies are needed to determine whether proteins in the nanoclusters are in the folded state upon dissociation of the nanoclusters to protein monomer. To determine whether irreversible protein aggregates are present in our 1B7 nanocluster dispersions at 267 mg/mL, we performed a battery of biophysical and biochemical tests. The dispersions were diluted several hours after formulation, as long-term storage stability is outside the scope of this work. (In practical applications, the dispersions could be formed and then injected into patients shortly thereafter.) However, the protein within the dispersion was stressed through viscosity testing earlier, as it was drawn through a 25 gauge needle, subjecting it to significant shear forces with a shear rate

TABLE 1. 1B7 Stability and Activity in Nanocluster Dispersion Samples with $c = c_E$ = 267 mg/mL Diluted to 1 mg/mL in PBS Prior to Analysis (Error Indicated Is ±SD)

sample	T_m (°C)[†]	% monomer (SEC)	EC_{50} (ELISA)
control solution	67.7 ± 0.3	98.88 ± 0.04	1.00 ± 0.24
diluted dispersion (from 267 mg/mL)	68.3 ± 0.3	98.59 ± 0.04	1.03 ± 0.20

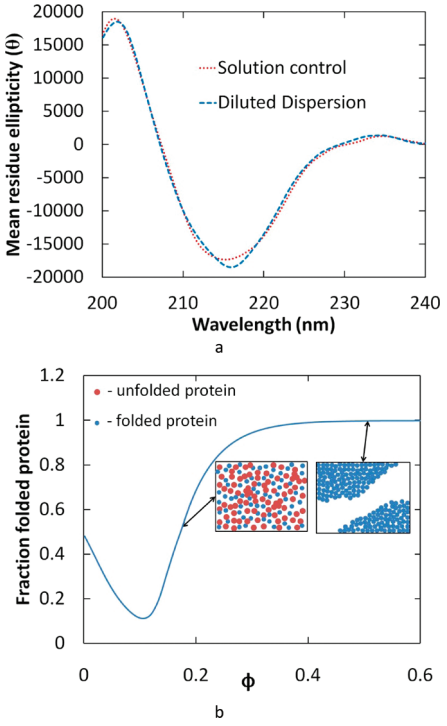

Figure 4. Antibody conformation and activity. (a) Circular dichroism spectra of monoclonal antibody 1B7 control and 267 mg/mL dispersion. All samples were diluted to 0.1 mg/mL in PBS and analyzed on a Jasco J-815 CD spectrometer. (b) Theoretical prediction of the fraction of folded protein suggesting that the native state would be favored at high ϕ_{int} = 0.6 found in antibody nanocluster (extended from Shen *et al.*[5]).

estimated to be as high as 9500 s^{-1} assuming a Newtonian fluid. Remarkably, after dilution to 1 mg/mL in PBS, we were unable to detect a change in protein conformation or activity relative to the control antibody in solution (Table 1). Prior to dispersion, analysis of a control 1B7 antibody solution in PBS exhibited a stability typical of monoclonal antibodies,[48] with an apparent thermal unfolding transition temperature (T_m) of 68 °C (Table 1) and an unfolding midpoint at 6.2 M urea. After dilution of the dispersion, the T_m was again measured to be 68 °C (Table 1). Since a T_m change of 2−3 degrees indicates a change in conformational stability, these data demonstrate that the average 1B7 thermal stability was not altered.[49] Circular dichroism (CD) was used to monitor the presence of secondary structure elements in the protein as a function of absorption of polarized light at particular wavelengths. Both the control solution and diluted dispersion retained the same strong negative signal

at 217 nm, indicative of the folded β-sheet structure characteristic of antibodies (Figure 4a and Table 2).[50] Table 2 shows the secondary structure as estimated by Dichroweb, using the CDSSTR fitting algorithm. It is generally accepted that a normalized root-mean-square deviation (nrmsd) of <0.1 indicates a good fit.[51] As shown in Table 2, the calculated percent β-sheet structure (the predominant secondary structure in antibodies) does not differ between the 1B7 control solution and the diluted dispersion.

Finally, two additional sizing methods were used to directly assess whether or not a small population of misfolded and larger molecular weight aggregates was present. As opposed to analysis of high concentration antibody solutions,[15] HPLC size exclusion chromatography (HPLC-SEC) and SDS-PAGE analyses of the diluted dispersions show a negligible increase in higher molecular weight aggregates when compared with the initial solution control (Table 1 and Figures S6 and S7 in Supporting Information). The presence of aggregates was also not apparent by DLS in the sharp monomer peaks (Figure 2a,c). HPLC size exclusion chromatography is able to discriminate antibody monomers from noncovalent and covalent aggregates, while nonreducing SDS-PAGE detects covalent multimers. Figure S6 in Supporting Information also shows the HPLC-SEC data for the intermediate steps in the dilution experiment for the 1B7 dispersion that are shown by DLS in Figure 2a,c. In all cases, there was not an increase in aggregates over the initial solution control.

Although these biophysical tests (SEC, DLS, CD, and SDS-PAGE) did not detect protein structural perturbations or aggregation, it is possible that the dispersed samples may have folded monomeric protein that does not retain biological activity. Thus, sensitive biological assays were used for determining activity that may be applied for protein concentrations <10 ng/mL. To monitor ligand-binding activity, indirect ELISAs using pertussis toxin as a capture molecule measured the 1B7 activity in terms of the relative 50% effective concentration ($EC_{50,disp}/EC_{50,control}$). This ratio is the concentration of antibody resulting in 50% of the maximum ELISA response for the dispersion (after dilution to 1 mg/mL) *versus* that for an unmodified control solution. Here, the diluted dispersion yielded a relative activity of 1.03 ± 0.20, which is indistinguishable from measurements made with the solution control (Table 1).[52] This result demonstrates that antigen binding ability, a powerful measure of protein activity, is identical for antibody recovered upon diluting a dispersion and a solution control.

The experimentally demonstrated stability of the native protein state in the large self-crowded nanoclusters may be anticipated from coarse-grain globular protein models[5,6] (Figure 4b). Specifically, for ultrahigh volume fractions of proteins within the nanoclusters ($\phi_{int} \sim 0.6$), the fraction of folded protein approaches unity. This reflects the entropic self-crowding (inset in Figures 4b and 1c,d) penalty for unfolding to more expanded non-native conformations, which overwhelms other factors (*e.g.*, the increase in both chain conformational entropy and favorable hydrophobic protein–protein interactions upon unfolding) that can otherwise destabilize the native state in less crowded environments. Importantly, the high ϕ_{int} within the clusters (>400 mg/mL) strongly favors the native state *via* self-crowding, even for overall ϕ values where proteins aggregate and unfold when in solutions without clusters.

TABLE 2. Estimation of 1B7 Secondary Structure from Circular Dichroism

sample	% α-helix	% β-strand	% turn and unordered	nrmsd[a]
control solution	0	39	63	0.006
diluted dispersion (from 267 mg/mL)	1	40	60	0.006

[a] Normalized root-mean-square deviations between the calculated and experimental CD spectra. The program CDSSTR was used for all secondary structure estimates *via* the Dichroweb online analysis.

Although protein stability and conformation were not measured experimentally within the nanoclusters, upon dilution, the proteins were clearly active, stable, and monomeric. Thus, irreversible aggregates were not present within the nanoclusters, despite the high protein concentrations. As discussed above, within the nanoclusters, the native conformation would be expected to be entropically stabilized by protein self-crowding. In addition, the relatively low mobility of the proteins in the clusters, given the high intracluster concentrations of ~700 mg/mL, may kinetically frustrate protein conformational changes that could otherwise lead to contact between hydrophobic patches and stabilize non-native complexes and aggregated states.

During these *in vitro* dilution experiments, the rapid dissolution (estimated at <1 ms; see Supporting Information) also lowers the probability of protein collisions that may otherwise produce irreversible aggregates. Immediately upon dilution, concentration and solubility gradients will result in release of antibody molecules from the nanocluster surface, while molecules buried within the cluster remain self-crowded, thus favoring stable folded protein within the cluster. This hypothesis is supported by the lack of an increase in the aggregates based on HPLC-SEC data and SDS-PAGE data upon dilution of the clusters, which decreases D_c, as is shown in Figures S6 and S7. Finally, the trehalose within the dispersion is present as the nanoclusters dissolve and thus favors folded protein.

Mechanism of Protein Assembly into Clusters. Assembly of nongelling dispersions of monodisperse protein nanoclusters relies on properly balancing hierarchical, multiscale interactions. Protein molecules should attract one another (favoring cluster formation), individual proteins should interact neutrally with the clusters[27]

(limiting cluster size), and nanoclusters should repel one another (avoiding gelation).

We begin by examining the potential of mean force between two proteins at the molecular level before discussing the nanoclusters. Figure 5a shows estimates for the contributions to the potential of mean force $V(r)$ for two 1B7 molecules (the parameters used in this case are given in Table S1 in Supporting Information). For pH 3 units away from pI, $V_{el}(r)$ is strongly repulsive. At these conditions, as should be expected, only very small clusters have been observed, as seen for lysozyme.[23] Near the pI, V_{el} becomes very weak, and thus with a strong V_{dep} for c_E = 220 mg/mL, $V(r)$ is attractive. This attraction may now be shown to drive formation of clusters, as described by the equilibrium free energy model.

To understand the cluster formation mechanism, consider an aqueous solution of protein and relatively concentrated crowder molecules at conditions near the protein's pI. Two protein molecules in this system will strongly attract one another because the magnitude of the electrostatic repulsion between the weakly charged monomers is vanishingly small compared to the short-range depletion attraction (Figures 1a and 5a). However, the interaction between a protein monomer and a *cluster* of proteins is more complex because the monomer feels, in addition to the short-range depletion attraction, the net effect of many weak, longer-ranged repulsions from the charged protein within the cluster. This interaction can be attractive or repulsive depending on the size of the cluster.[27,28] If the cluster is sufficiently large, then these repulsions balance the depletion attraction, limiting further cluster growth (Figure 1a). The equilibrium cluster size increases with increasing strength of depletion interactions between the protein monomers (*e.g.*, with increasing crowder concentration) and decreases with the increasing strength of the repulsive interactions (*e.g.*, with number pH units away from the pI). Because of their collective electrostatic repulsions, it will be shown that fully grown clusters in solution do not attract one another.

The contours for protein cluster diameters, D_c, shown in Figure 5b were computed from an extension of a simple equilibrium free energy model[27,28] which has previously been applied to understand clustering of polymeric colloids in organic solvents.[25] In that model, D_c is determined by a balance between short-range interparticle attractions and weak, longer-range electrostatic repulsions.

To understand the equilibrium model, consider n_c proteins of radius R that form a cluster of radius R_c in solution, as shown in Figure 1a. In our analysis, the only attraction we explicitly consider is the crowder-mediated depletion interactions, which (as explained above) is the dominant attractive interaction under strong clustering conditions. If the depletion interaction between two proteins is $-\varepsilon$, and each protein has C nearest neighbors in the cluster interior, then the effective depletion contribution to the free energy per

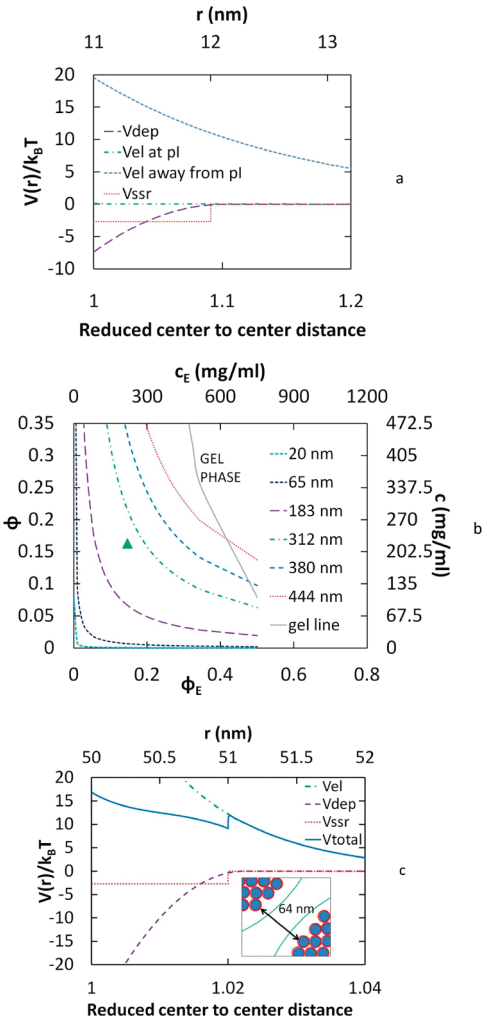

Figure 5. Protein−protein, protein−cluster, and cluster−cluster hierarchical interactions in nanocluster dispersions. The potential of mean force includes specific short-ranged (ssr), depletion attraction (dep), and electrostatic (el) components: $V(r) = V_{ssr}(r) + V_{dep}(r) + V_{el}(r)$. (a) Components of $V(r)$ for protein monomers at pI and 3 pH units away from pI. (b) Predicted cluster diameter contours. The green triangle denotes the conditions of the injected dispersion into mice at c = 235 mg/mL for 1B7 as given in Table S3 in Supporting Information. The diagonal pathway represents dilution of the dispersion (Figure 2a). (c) $V(r)$ for two 50 nm nanoclusters based on experimental ζ-potential for polyclonal IgG (Supporting Information). Inset: green arc depicts range of long-ranged repulsion at the edges of two clusters, and red indicates short-ranged intercluster attraction.

protein molecule in the cluster interior will be $-\varepsilon C/2$. The "missing" depletion interactions for proteins on the cluster surface are accounted for by adding an effective surface energy term ($4\pi R_c^2\gamma$), where the surface tension is approximated as $\gamma = \varepsilon/4\pi R^2$. In other words, the depletion attractions contribute the following to the cluster free energy

$$F_{att} = -\frac{\varepsilon C n_c}{2} + 4\pi R_c^2 \gamma \qquad (1)$$

Assuming that the charges are negligibly screened within the cluster (as discussed in Supporting Information),

their repulsive self-energy can be approximated by that of a uniform distribution of point charges in a spherical volume with the cluster radius R_c

$$F_{rep} = \frac{3\lambda k_B T n_c^2 q^2}{5R_c} \quad (2)$$

where λ is the Bjerrum length ($\lambda = e^2/4\pi\varepsilon_r\varepsilon_0 k_B T$), ε_r is the relative permittivity of the medium, and q is the charge per protein. The minimization of the $F = F_{att} + F_{rep}$ with respect to R_c (or n_c) gives

$$n_c = \frac{10\pi\gamma R^3}{3k_B T\lambda q^2} \quad (3)$$

This simple result illustrates that the equilibrium n_c increases with attraction and decreases with electrostatic repulsion.

To further understand the cluster free energy in terms of the translational and combinatorial entropy of the counterions dissociating from the protein molecules, it is to instructive to write[27]

$$F_{entropic} = 2n_c q\left[\ln\left(\frac{q}{q_0}\right) - 1\right] \quad (4)$$

The quantity q_0 represents the charge per protein q that minimizes the overall cluster free energy (see also eq 5 below) for conditions corresponding to very low values of ζ-potential (where $\lambda/R_c \rightarrow 0$; *i.e.*, the weakly charged systems of interest here). It can be expressed as

$$q_0 = (4\pi n_d/3\phi)^{1/2}(R/b)^{3/2}e^{-\lambda/(2b-1)} \quad (5)$$

where n_d is the number of dissociable sites on a protein surface, b is the distance of closest approach between a counterion and a charge on the protein surface, and ϕ is the volume fraction of proteins in solution. As discussed extensively elsewhere,[27] higher values of ϕ generally result in lower q_0 because, with more proteins present in the system, fewer counterions per protein need to dissociate to achieve the same increase in counterion translational entropy. Combining terms, the free energy per protein of a cluster given by[28]

$$\frac{f_c}{k_B T} = -\frac{\varepsilon C}{2k_B T} + \frac{4\pi R_c^2\gamma}{k_B T n_c} + \frac{3\lambda n_c q^2}{5R_c} + 2q\left[\ln\left(\frac{q}{q_0}\right) - 1\right] \quad (6)$$

To take into account the porosity of the protein cluster, we modify the original model by expressing the cluster radius as

$$R_c = \left(\frac{n_c}{k}\right)^{1/\delta_f} R \quad (7)$$

where δ_f is the fractal dimension (2.6 from Figure S3 in Supporting Information) and k is a constant chosen as unity. The resulting modified free energy equation is

$$\frac{f_c}{k_B T} = -\frac{\varepsilon C}{2k_B T} + \frac{\varepsilon n_c^{(2/\delta_f - 1)}}{k_B T k^{2/\delta_f}} + \frac{3\lambda n_c^{(1 - 1/\delta_f)} q^2}{5R_c k^{1/\delta_f}} + 2q\left[\ln\left(\frac{q}{q_0}\right) - 1\right] \quad (8)$$

Minimizing f_c with respect to n_c at $q = q_0$ gives the following estimate for the equilibrium aggregation number (n^*)

$$n^* = k^{3/(3-2\delta_f)}\left\{\frac{5(\delta_f - 2)\varepsilon R}{3(\delta_f - 1)k_B T\lambda q_0^2}\right\}^{\delta_f/(2\delta_f - 3)} \quad (9)$$

As should be expected, the cluster size increases with increased strength of the attraction, ε. Since we are interested here in cases where V_{ssr} (hydrogen bonding, hydrophobic interactions, *etc.*) is smaller in magnitude than the crowder-mediated depletion attraction (Figure 5a), we approximate ε as the contact value of the depletion potential in eq S2 in Supporting Information [$-\varepsilon(\phi_E, R/R_E) = V_{dep}(r = 2R)$]. In the limit of solid clusters with $\delta_f = 3$, eq 9 becomes eq 3, which is essentially the same as eq 23 in Groenewold and Kegel.[27] The only difference is in the coefficient which is explained elsewhere.[53]

Table S2 in Supporting Information summarizes our input variables for the model to determine the R_c contours in Figure 5b. The R_c is determined from setting n^* from eq 9 into eq 7. The total number of dissociable sites on the protein monomer at a given pH, n_d, was chosen as 50 based on previous estimates.[50] The fractal dimension is chosen as 2.6 based on the SEM images and SLS measurements (Figure S3 in Supporting Information). The ε_r inside the clusters was chosen as 25 as explained in detail in Supporting Information. The distance between opposite charges in an ionic bond is taken to be ~0.1 nm, and the protein diameter is 11 nm (Table S2 in Supporting Information).[54]

The effects of ϕ and ϕ_E on R_c are illustrated in Figure 5b from the equilibrium model for clustering of colloids,[27,28] which has been extended to account for the fractal dimension of the cluster (see eq 9). We assumed based on Figure 5a that short-range attractive interactions between proteins are dominated by depletion attractions (eq S2 in Supporting Information) at high values of ϕ_E as is evident at contact. This attraction is balanced by weak long-ranged repulsions with negligible electrostatic screening *within* the dense clusters (see Supporting Information). On a horizontal pathway in Figure 5b, increasing ϕ_E at fixed ϕ strengthens V_{dep} (crowding) and hence increases R_c. This pathway raises the depletion attraction between protein monomers (higher ε) and therefore the numerator in eq 9 (and likewise eq 3) which increases R_c. The predictions of the model are in reasonable agreement with experimental data as shown in Figure 2b,d, where the cluster size increases with an increase in the c_E. In addition, on a vertical pathway increasing ϕ at

fixed ϕ_E lowers the charge per protein in the cluster because fewer counterions *per protein* must dissociate to obtain the same balance between entropy and energy in the system,[27] which also increases R_c. For the combined change whereby ϕ and ϕ_E decrease upon dilution along a diagonal slant, R_c decreases (Figure 5b). Here both the decrease in depletion attraction and the lower ϕ and its effect on charge produce a decrease in R_c. Again, this prediction is in agreement with the experimental data as shown in Figure 2a−d. Our new model, as well as the one it is based on,[27,28] is only meant to provide qualitative predictions. The model does not consider intracluster charge screening, differences in ε_r inside and outside the cluster, and variations in the attractive interaction with r. However, the simple equilibrium model substantiates the novel experimental discovery of reversible equilibrium nanoclusters and qualitatively predicts the experimental trends in D_c.

In contrast to the predominantly attractive interactions between individual proteins near their pI in Figure 5a, the resulting nanocluster interactions are highly repulsive (Figure 5c). The dominance of intercluster repulsions is due to the large number of weakly charged proteins per cluster (>1000 proteins/cluster and ~1 elementary charge/protein) and the longer range of V_{el} (eq S5 in Supporting Information) which scales as R_c. In contrast, the range of V_{dep} and V_{ssr} (eqs S2 and S3 in Supporting Information) is <1 nm and thus almost negligible *versus* the intercluster spacing (Figure 5c inset).

Under conditions for which the electrostatic repulsion is insufficient to balance the attractive forces (*i.e.*, very high crowder or protein concentrations), the protein can also form a gel.[21] The spinodal instability associated with this transition in the context of the clustering model[28] can be defined as the locus of points where $d^2f_{cl}/dq^2 = 0$ (see gray line in Figure 5b). Note that equilibrium clusters with various sizes may be formed before the gel phase boundary, according to the experimental data and the theoretical cluster size contours.

Viscosity of Nanocluster Dispersions. The very weak attraction between clusters led to a viscosity of the dispersion of 1B7 at c = 267 mg/mL of only 40 cP which is a syringeable value (Table 3 and video in Supporting Information). Similarly, it was 63 cP for polyclonal sheep IgG at c = 275 mg/mL. The viscosity of the dispersion is commonly described as a function of the intrinsic viscosity, $[\eta]$, maximum volume fraction of particles, ϕ_{max}, and the solvent viscosity (including extrinsic crowder), η_0, using the Krieger−Dougherty equation[55,56]

$$\frac{\eta}{\eta_0} = \left[1 - \left(\frac{\phi_{eff}}{\phi_{max}}\right)\right]^{-[\eta]\phi_{max}} \quad (10)$$

η may be reduced by lowering η_0, or $[\eta]$, which is a minimum of 2.5 for hard sphere colloids. We chose ϕ_{max} = 0.64, the value for "maximally" random packed spheres.[57] The value of effective cluster volume fraction ϕ_{eff} was defined as ϕ/ϕ_{int}, on the basis of the ϕ_{int} from SLS, ~0.6. From eq 10, $[\eta]$ for both 1B7 and IgG clusters was found to be ~7. At the present time, the variation of ϕ_{int} with nanocluster size is not well understood, thus we assumed a constant value of ϕ_{int} of 0.6, and therefore, the values of ϕ_{eff} are only approximate.[58] If ϕ_{int} was lower, then the larger ϕ_{eff} would lead to an even smaller $[\eta]$. In the future, SAXS may be used to better understand the cluster morphology.[59] Higher $[\eta]$ values of 11−20 are often observed for monoclonal antibody solutions.[60] Similarly, we observed for monomeric IgG (without trehalose as an extrinsic crowder) an $[\eta]$ of 18 at c = 260 mg/mL (Table 3). Finally, at c = 300 mg/mL, again for c_E = 0, the viscosity of the IgG solution was found to be not measurable as the solution was in the form of a gel that did not flow. This gelation was a manifestation of the high $[\eta]$ in solution resulting from attraction between the protein molecules with small spacings. In contrast, the nanocluster dispersions did flow at this c with $c = c_E$, with a viscosity of 250 cP. In principle, this viscosity may be lowered by optimizing the composition of the extrinsic crowder.

***In Vivo* Study of Protein Stability and Pharmacokinetics in Mice.** To test the potential for drug delivery of protein nanocluster dispersions, we performed an *in vivo* pharmacokinetics (PK) study in mice. Control groups received 100 μL of dilute antibody solution *via* intraveneous or subcutaneous injection to provide a baseline defined as full bioavailability. Using a highly concentrated 235 mg/mL nanocluster dispersion, 1 μL was injected subcutaneously at pH 7.2 (Table 4). The viscosity of this dispersion was well below 40 cP (see Table 3), which is below the typical limit of 50 cP for subcutaneous injection. Remarkably, the resulting PK parameters, including normalized bioavailability (AUC/dose), $C_{max/dose}$, t_{max}, and elimination kinetics, were statistically indistinguishable from those of the two subcutaneous groups (Figure 6). The similar bioavailabilities suggest that the antibody molecules in the nanoclusters readily dissociated (the predicted time in buffer is 7 ms, eq S10 in Supporting Information) were transported from the injection site and entered the bloodstream, while identical α and β rates indicate the presence of predominantly monomeric antibody in the blood. If the antibodies were to aggregate or misfold during dissolution, the molecular weight and surface properties would change, in turn affecting renal and hepatic clearance rates.[47] Finally, analysis of antibody activity in the terminal blood samples with an *in vitro* toxin neutralization test showed similar activities *versus* control antibody, indicating that, in addition to antibody conformation, activity was unaffected. It is likely this nanocluster drug delivery concept could be extended to even higher dosages, given that dispersion concentrations up to 400 mg/mL for BSA and 350 mg/mL for polyclonal IgG were attained (Figure 3 and Figure S5 in Supporting Information). Whereas these tests provide a preliminary indication that the

TABLE 3. Viscosity and Hydrodynamic Diameter for Monoclonal 1B7 Antibody and Polyclonal Sheep IgG Dispersions

protein concentration (c, mg/mL)	trehalose concentration (c_E, mg/mL)	Viscosity (η, cP)	ϕ_{eff}	intrinsic viscosity ([η])	hydrodynamic diameter	hydrodynamic diameter standard deviation
267 (1B7)	270	40	0.32	7.2	315	17
275 (IgG)	275	63	0.33	7.9	88.0	9.0
260 (IgG)	0	57	0.19	18	9.66	1.84

TABLE 4. Pharmacokinetic parameters for curves shown in Fig. 6. Error is ± s.d

Formulation	C_{max}/ dose (μg/mL)/(mg/kg)	$AUC_{0-\infty}$/ dose (μg·hr/ml)/(mg/kg)	t_{max} (hrs)	$t_{1/2,\alpha}$ (hrs)	$t_{1/2,\beta}$ (hrs)	Relative neutralization titer
IV solution	25.5 ± 3.8	3582 ± 990	15.1 ± 0.7	45.7 ± 22.8	227.1 ± 24.9	2.3 ± 1.7
SQ solution	18.8 ± 4.4	2699 ± 583	18.9 ± 3.1	43.4 ± 17.3	210.0 ± 17.4	1.0 ± 1.8
SQ nanocluster dispersion	14.3 ± 3.1	3269 ± 291	21.4 ± 2.9	42.1 ± 24.8	243.2 ± 35.5	1.3 ± 0.5

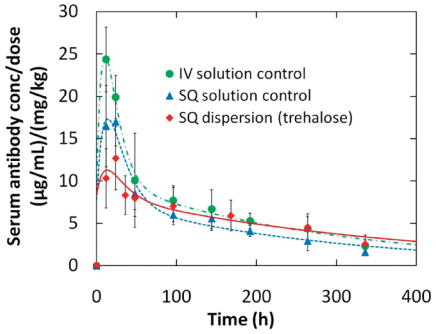

Figure 6. Pharmacokinetics of concentrated 1B7 dispersion and solution controls. Time course of serum antibody concentration normalized by dose after administration of intravenous solution, subcutaneous solution, or subcutaneous dispersion. Serum samples were recovered from the tail vein and the 1B7 concentration determined by ELISA.

nanoclusters may potentially be used for subcutaneous delivery, further work is needed to address various practical questions beyond the scope of this study. For example, the dispersions could be formed by mixing powder and buffer and then injected soon thereafter to avoid the need for long-term storage stability. For proteins with an isoelectric point more than 2 units away from physiological pH, this approach may require even greater concentrations of crowder to overcome electrostatic repulsion, or eventually may not be practical.

CONCLUSIONS

Low viscosity dispersions of concentrated protein in monodisperse equilibrium nanoclusters, with high conformational stability *in vitro* and high biological activity *in vivo* upon dilution, have been formed simply by mixing lyophilized protein, an extrinsic crowder and buffer. The high degree of self-crowding of the protein within the nanoclusters at an unusually high concentration of 700 mg/mL is shown theoretically to favor folding, as confirmed experimentally upon dilution of 1B7 nanoclusters. The size of the nanoclusters is tunable by adjusting the protein and extrinsic crowder concentrations near the pI, as shown both experimentally and with a free energy model. The ability to simultaneously achieve self-crowded clusters and low viscosities results from a general concept of tuning the multiscale interactions with attraction dominant at the protein monomer level, repulsion at the intercluster level, and a neutral balance of the two for the monomer−cluster interaction. The intercluster repulsion favors colloidal stability and low viscosity without gelation. Remarkably, an analysis with a variety of physical, chemical, and biological assays indicated conformationally stable protein monomer without any loss of protein activity after dilution of the nanocluster dispersions. *In vivo* subcutaneous administration of dispersed antibody resulted in indistinguishable pharmacokinetics and activity compared to control antibody solutions. This general approach for formulating dispersions of protein nanoclusters with crowding agents and a pH near the isoelectric point offers the potential of subcutaneous administration of a variety of therapeutic biologics, which would otherwise gel when formulated as solutions.

METHODS

Formation of Nanocluster Dispersion. The murine IgG2a antibody 1B7 was expressed, purified, and characterized as previously reported,[45] and the pI determined *via* silver-stained isoelectric focusing gel. Prior to lyophilization, the 1B7 solution was buffer exchanged into a 20 mM histidine buffer (pH 5.5) using a 50 000 molecular weight cutoff (MWCO) Centricon filter and solid α, α-trehalose added to a 1:1 protein/trehalose weight ratio as a cryoprotectant. The solution was filter-sterilized (0.22 μm), diluted to 20 mg/mL protein with 20 mM histidine buffer (pH 5.5), and transferred to a sterile 8 mL glass vial. It was frozen over 6 h on a precooled lyophilizer tray at −40 °C (VirTis Advantage Plus Benchtop Freeze-Dryer) and then lyophilized at 150 mTorr with 12 h of primary drying at −40 °C followed by a 6 h ramp to 25 °C and an additional 6 h of secondary drying at 25 °C. To create a dispersion, typically 28 ± 0.02 mg of

lyophilized protein was compacted into a tared 0.1 mL conical vial (Wheaton Science Products). After addition of 50 mM sodium phosphate buffer (pH 7.2), the resulting dispersion was stirred gently with the tip of a 25 gauge needle. The total volume and volume fractions of the components were calculated assuming ideal mixing based on known masses and hypothetical pure liquid protein (1.35 g/cm^3) and trehalose (1.64 g/cm^3) densities, from their partial molar volumes at infinite dilution[61,62] and a known buffer volume. The final protein concentration was verified using a BCA assay or light absorbance at 280 nm with a mass extinction coefficient of 1.37 L/g·cm (Nanodrop, Thermo Scientific) to be within experimental error of the predicted value.

Characterization of the Nanocluster Dispersions. The hydrodynamic diameters of protein monomers and nanoclusters were measured by dynamic light scattering (DLS) with a 632.8 nm (red) laser and an avalanche photodiode at ~23 °C using CONTIN (Brookhaven BI-9000AT). The scattering angles ranged from 135 to 165° to minimize multiple scattering[43] with the use of a 60 μL sample cell (Beckman Coulter). In order to verify the accuracy of this technique, the hydrodynamic diameter of a 298 nm polystyrene standard was measured at $\phi \sim 0.1$ and found to be within 5% of the actual size. The scattering measurements for each sample of protein monomer or nanocluster were done at two separate angles consisting of 135, 150, or 165°, and the size was found to be within 5−10% for the two angles. According to a study of DLS and rheology of concentrated colloids, the calculation of the hydrodynamic diameter from the Stokes−Einstein equation based on the solvent viscosity is relatively accurate at our highest ϕ of 0.25.[43] At higher ϕ values, interactions between particles during the time scale of the measurement may produce much larger deviations from the Stokes−Einstein equation. To avoid these complexities, the particle size may be determined from small-angle X-ray scattering (SAXS).[59] For determining the fractal dimension of the IgG nanoclusters (Figure S3 in Supporting Information), the scattered laser light intensity was measured at scattering angles every 5° between 45 and 90° using a cylindrical 2 mL capacity ampule.

To prepare samples for scanning electron microscopy (SEM, Hitachi S-5500 at 30 KV), the dispersions were diluted to 40 mg/mL at a constant crowder volume fraction of 0.18 (corresponding to original dispersion at 220 mg/mL) using PEG-300 as a crowder, placed on a copper TEM grid with a carbon film coated with Formvar, blotted to remove the excess liquid, rapidly frozen by immersion in liquid nitrogen, and lyophilized. The viscosity of the nanocluster dispersions was measured in triplicate using a 25 gauge (i.d. = 0.1 mm) 1.5 in. long needle attached to a 1 mL syringe, according to the Hagen-Pouiselle equation. The time to draw the dispersion from a height from the bottom of the cone from 0.4 to 0.1 in., corresponding to a volume of ~50 μL, was determined from analysis of a digital video (see movie in Supporting Information).[56] A linear correlation between the time to draw 0.05 mL from the conical vial and the viscosity of various calibration fluids is shown in Figure S8 in Supporting Information.[56,63] The shear rate decreased with the viscosity and was 1000 s^{-1} at a viscosity of 50 cP. The viscosities of trehalose solutions were calculated from Uchida *et al.*[64]

Characterization of the Protein Structure and Activity. To monitor antibody structure and ligand-binding activity, lyophilized and dispersed protein were diluted to 1 mg/mL in PBS, prior to analysis by a battery of biophysical and biochemical assays *versus* solution control antibody. Typically, the dilution was performed within ~4−6 h of the formation of the dispersion. Circular dichroism (CD) measurements were collected from 260 to 185 nm in 0.1 nm steps using a Jasco J-815 CD spectrometer. The formation of insoluble and disulfide-linked aggregates was monitored by analysis of 5 μg samples of dilute protein on a 4−20% nonreducing SDS-PAGE gel. Formation of noncovalent aggregates was monitored by SEC, with 20 μg of diluted dispersion analyzed with a Waters Breeze HPLC. To analyze ligand-binding activity, an indirect PTx ELISA was performed as previously described[46] and reported as the ratio of 50% effective concentration values (EC_{50}) for the sample *versus* solution control. The thermal melting temperature (T_m) was quantified with using a 7900HT thermocycler from Applied Biosystems and SYPRO orange protein gel stain (Sigma-Aldrich).[44]

***In Vivo* Bioavailability in BALB/c Mice.** An *in vivo* pharmacokinetic study of the 1B7 dispersion and a control solution was performed over a 14 day period using 24−27 g female BALB/c mice. The three sample groups included (1) intravenous (IV) and (2) subcutaneous (SQ) control injections of 100 μL of a dilute 1B7 solution and (3) a test condition, SQ injection of an antibody dispersion (235 mg/mL in a 1 μL volume to yield a 9.4 mg/kg dose). Prior to injection and at eight additional time-points between 12 and 336 h, serum samples (~20 μL) were collected from the tail vein. At the terminal time-point, mice were anaesthetized and serum was collected by cardiac puncture. This study was performed with approval by the Institutional Animal Care and Use Committee at the University of Texas at Austin (protocol #AUP-2010−00070) in compliance of guidelines from the Office of Laboratory Animal Welfare. To determine the concentration of active 1B7 in each serum sample, an indirect PTx ELISA was performed as previously described.[45] Each plate included mouse serum (Sigma) as a negative control and a 1B7 standard curve diluted in mouse serum. SoftMax Pro v5 was used to calculate EC_{50} values based on the serum dilution using a 4 parameter logistic (4PL) model and total concentrations of active 1B7 present in serum samples calculated from the standard curve. An orthogonal antibody activity assay, based on *in vitro* CHO cell neutralization of PTx, was performed using serum from the terminal time-point.[45]

Conflict of Interest: The authors declare the following competing financial interest(s):We have a competing financial interest in patent applications.

Acknowledgment. We acknowledge support from the Packard Foundation (#29098, JAM), Welch Foundation (F-1319, K.P.J.; F-1696, T.M.T.), National Science Foundation (NSFSTC-CHE-9876674, K.P.J.; CBET-0968038, K.P.J.; CBET-1065357, T.M.T.), and Gates Foundation (J.A.M.). We thank E. Cho at Texas Institute for Drug and Diagnostic Development (TI-3D) for CD spectra, D. Slanac for SEM, and E. Zumalt at Cockrell School of Engineering Faculty Innovation Center for the artistic schematic.

Supporting Information Available: Potential of mean force between protein molecules and protein nanoclusters; surface and ζ-potential of protein nanoclusters and discussion; explanation of low effective dielectric within the clusters; dissolution time of protein nanoclusters; additional SEM images of protein nanoclusters; static light scattering for cluster fractal dimension; additional examples of clusters with polyclonal sheep IgG; HPLC SEC, SDS-PAGE, and additional data to prove the presence of monomeric protein; viscosity calibration data; parameters used in theoretical calculations for cluster sizes and potentials; movie for viscosity measurements. This material is available free of charge *via* the Internet at http://pubs.acs.org.

REFERENCES AND NOTES

1. Hartl, F. U.; Hayer-Hartl, M. Protein Folding—Molecular Chaperones in the Cytosol: From Nascent Chain to Folded Protein. *Science* **2002**, *295*, 1852–1858.
2. Zhou, H. X.; Rivas, G.; Minton, A. P. Macromolecular Crowding and Confinement: Biochemical, Biophysical, and Potential Physiological Consequences. *Annu. Rev. Biophys.* **2008**, *37*, 375–397.
3. Davis-Searles, P. R.; Saunders, A. J.; Erie, D. A.; Winzor, D. J.; Pielak, G. J. Interpreting the Effects of Small Uncharged Solutes on Protein-Folding Equilibria. *Annu. Rev. Biophys. Biomol. Struct.* **2001**, *30*, 271–306.
4. Hall, D.; Minton, A. P. Macromolecular Crowding: Qualitative and Semiquantitative Successes, Quantitative Challenges. *Biochim. Biophys. Acta* **2003**, *1649*, 127–139.
5. Shen, V. K.; Cheung, J. K.; Errington, J. R.; Truskett, T. M. Coarse-Grained Strategy for Modeling Protein Stability in Concentrated Solutions II: Phase Behavior. *Biophys. J.* **2006**, *90*, 1949–1960.

6. Cheung, J. K.; Truskett, T. M. Coarse-Grained Strategy for Modeling Protein Stability in Concentrated Solutions. *Biophys. J.* **2005**, *89*, 2372–2384.
7. Cheung, M. S.; Klimov, D.; Thirumalai, D. Molecular Crowding Enhances Native State Stability and Refolding Rates of Globular Proteins. *Proc. Natl. Acad. Sci. U.S.A.* **2005**, *102*, 4753–4758.
8. Dhar, A.; Samiotakis, A.; Ebbinghaus, S.; Nienhaus, L.; Homouz, D.; Gruebele, M.; Cheung, M. S. Structure, Function, and Folding of Phosphoglycerate Kinase Are Strongly Perturbed by Macromolecular Crowding. *Proc. Natl. Acad. Sci. U.S.A.* **2010**, *107*, 17586–17591.
9. Kendrick, B. S.; Carpenter, J. F.; Cleland, J. L.; Randolph, T. W. A Transient Expansion of the Native State Precedes Aggregation of Recombinant Human Interferon-Γ. *Proc. Natl. Acad. Sci. U.S.A.* **1998**, *95*, 14142–14146.
10. Krishnan, S.; Chi, E. Y.; Webb, J. N.; Chang, B. S.; Shan, D.; Goldenberg, M.; Manning, M. C.; Randolph, T. W.; Carpenter, J. F. Aggregation of Granulocyte Colony Stimulating Factor under Physiological Conditions: Characterization and Thermodynamic Inhibition. *Biochemistry* **2002**, *41*, 6422–6431.
11. Stagg, L.; Zhang, S.-Q.; Cheung, M. S.; Wittung-Stafshede, P. Molecular Crowding Enhances Native Structure and Stability of Alpha/Beta Protein Flavodoxin. *Proc. Natl. Acad. Sci. U.S.A.* **2007**, *104*, 18976–18981.
12. O'Connor, T.; Debenedetti, P.; Carbeck, J. Stability of Proteins in the Presence of Carbohydrates; Experiments and Modeling Using Scaled Particle Theory. *Biophys. Chem.* **2007**, *127*, 51–63.
13. Pielak, G. J.; Miklos, A. C. Crowding and Function Reunite. *Proc. Natl. Acad. Sci. U.S.A.* **2010**, *107*, 17457–17458.
14. Shire, S. J.; Shahrokh, Z.; Liu, J. Challenges in the Development of High Protein Concentration Formulations. *J. Pharm. Sci.* **2004**, *93*, 1390–1402.
15. Scherer, T. M.; Liu, J.; Shire, S. J.; Minton, A. P. Intermolecular Interactions of Igg1Monoclonal Antibodies at High Concentrations Characterized by Light Scattering. *J. Phys. Chem. B* **2010**, *114*, 12948–12957.
16. Zaccarelli, E. Colloidal Gels: Equilibrium and Non-Equilibrium Routes. *J. Phys.: Condens. Matter* **2007**, *19*, 323101.
17. Rosenbaum, D. F.; Zamora, P. C.; Zukoski, C. F. Phase Behavior of Small Attractive Colloidal Particles. *Phys. Rev. Lett.* **1996**, *76*, 150–153.
18. ten Wolde, P. R.; Frenkel, D. Enhancement of Protein Crystal Nucleation by Critical Density Fluctuations. *Science* **1997**, *277*, 1975–1978.
19. Fields, G. B.; Alonso, D. O. V.; Stigter, D.; Dill, K. A. Theory for the Aggregation of Proteins and Copolymers. *J. Phys. Chem.* **1992**, *96*, 3974–3981.
20. Young, T. M.; Roberts, C. J. Structure and Thermodynamics of Colloidal Protein Cluster Formation: Comparison of Square-Well and Simple Dipolar Models. *J. Chem. Phys.* **2009**, *131*, 125104.
21. Lu, P. J.; Zaccarelli, E.; Ciulla, F.; Schofield, A. B.; Sciortino, F.; Weitz, D. A. Gelation of Particles with Short-Range Attraction. *Nature* **2008**, *453*, 499–503.
22. Lu, P. J.; Conrad, J. C.; Wyss, H. M.; Schofield, A. B.; Weitz, D. A. Fluids of Clusters in Attractive Colloids. *Phys. Rev. Lett.* **2006**, 96.
23. Stradner, A.; Sedgwick, H.; Cardinaux, F.; Poon, W. C. K.; Egelhaaf, S. U.; Schurtenberger, P. Equilibrium Cluster Formation in Concentrated Protein Solutions and Colloids. *Nature* **2004**, *432*, 492–495.
24. Gast, A. P.; Hall, C. K.; Russel, W. B. Polymer-Induced Phase Separations in Nonaqueous Colloidal Suspensions. *J. Colloid Interface Sci.* **1983**, *96*, 251–267.
25. Sedgwick, H.; Egelhaaf, S. U.; Poon, W. C. K. Clusters and Gels in Systems of Sticky Particles. *J. Phys.: Condens. Matter* **2004**, *16*, S4913–S4922.
26. Pan, W. C.; Vekilov, P. G.; Lubchenko, V. Origin of Anomalous Mesoscopic Phases in Protein Solutions. *J. Phys. Chem. B* **2010**, *114*, 7620–7630.
27. Groenewold, J.; Kegel, W. K. Anomalously Large Equilibrium Clusters of Colloids. *J. Phys. Chem. B* **2001**, *105*, 11702–11709.
28. Groenewold, J.; Kegel, W. K. Colloidal Cluster Phases, Gelation and Nuclear Matter. *J. Phys.: Condens. Matter* **2004**, *16*, S4877–S4886.
29. Porcar, L.; Falus, P.; Chen, W.-R.; Faraone, A.; Fratini, E.; Hong, K.; Baglioni, P.; Liu, Y. Formation of the Dynamic Clusters in Concentrated Lyoszyme Protein Solutions. *J. Phys. Chem. Lett.* **2010**, *1*, 126–129.
30. Tam, J. M.; Murthy, A. K.; Ingram, D. R.; Nguyen, R.; Sokolov, K. V.; Johnston, K. P. Kinetic Assembly of Near-IR-Active Gold Nanoclusters Using Weakly Adsorbing Polymers To Control the Size. *Langmuir* **2010**, *26*, 8988–8999.
31. Tam, J. M.; Tam, J. O.; Murthy, A.; Ingram, D. R.; Ma, L. L.; Travis, K.; Johnston, K. P.; Sokolov, K. V. Controlled Assembly of Biodegradable Plasmonic Nanoclusters for Near-Infrared Imaging and Therapeutic Applications. *ACS Nano* **2010**, *4*, 2178–2184.
32. Xia, Y. S.; Nguyen, T. D.; Yang, M.; Lee, B.; Santos, A.; Podsiadlo, P.; Tang, Z. Y.; Glotzer, S. C.; Kotov, N. A. Self-Assembly of Self-Limiting Monodisperse Supraparticles from Polydisperse Nanoparticles. *Nat. Nanotechnol.* **2011**, *6*, 580–587.
33. Ping, G.; Yang, G.; Yuan, J.-M. Depletion Force from Macromolecular Crowding Enhances Mechanical Stability of Protein Molecules. *Polymer* **2006**, *47*, 2564–2570.
34. Minton, A. P. Adsorption of Globular Proteins on Locally Planar Surfaces. II. Models for the Effect of Multiple Adsorbate Conformations on Adsorption Equilibria and Kinetics. *Biophys. J.* **1999**, *76*, 176–187.
35. del Alamo, M.; Rivas, G.; Mateu, M. G. Effect of Macromolecular Crowding Agents on Human Immunodeficiency Virus Type 1 Capsid Protein Assembly *in Vitro*. *J. Virol.* **2005**, *79*, 14271–14281.
36. Lee, J. C.; Timasheff, S. N. The Stabilization of Proteins by Sucrose. *J. Biol. Chem.* **1981**, *256*, 7193–7201.
37. Chi, E. Y.; Krishnan, S.; Kendrick, B. S.; Chang, B. S.; Carpenter, J. F.; Randolph, T. W. Roles of Conformational Stability and Colloidal Stability in the Aggregation of Recombinant Human Granulocyte Colony-Stimulating Factor. *Protein Sci.* **2003**, *12*, 903–913.
38. Asakura, S.; Oosawa, F. Interaction between Particles Suspended in Solutions of Macromolecules. *J. Polym. Sci.* **1958**, *33*, 183–192.
39. Vrij, A. Polymer at Interfaces and Interactions in Colloidal Dispersions. *Pure Appl. Chem.* **1976**, *48*, 471–483.
40. Mutch, K. J.; van Duijneveldt, J. S.; Eastoe, J. Colloid-Polymer Mixtures in the Protein Limit. *Soft Matter* **2007**, *3*, 155.
41. Sharma, A.; Walz, J. Y. Direct Measurement of the Depletion Interaction in a Charged Colloidal Dispersion. *J. Chem. Soc., Faraday Trans.* **1996**, *92*, 4997–5004.
42. Tuinier, R.; Vliegenthart, G. A.; Lekkerkerker, H. N. W. Depletion Interaction between Spheres Immersed in a Solution of Ideal Polymer Chains. *J. Chem. Phys.* **2000**, *113*, 10768–10775.
43. Horn, F. Hydrodynamic and Colloidal Interactions in Concentrated Charge-Stabilized Polymer Dispersions. *J. Colloid Interface Sci.* **2000**, *225*, 166–178.
44. Lavinder, J. J.; Hari, S. B.; Sullivan, B. J.; Magliery, T. J. High-Throughput Thermal Scanning: A General, Rapid Dye-Binding Thermal Shift Screen for Protein Engineering. *J. Am. Chem. Soc.* **2009**, *131*, 3794–3795.
45. Sutherland, J. N.; Maynard, J. A. Characterization of a Key Neutralizing Epitope on Pertussis Toxin Recognized by Monoclonal Antibody 1B7. *Biochemistry* **2009**, *48*, 11982–11993.
46. Sutherland, J. N.; Chang, C.; Yoder, S. M.; Rock, M. T.; Maynard, J. A. Antibodies Recognizing Protective Pertussis Toxin Epitopes Are Preferentially Elicited by Natural Infection *versus* Acellular Immunization. *Clin. Vaccine Immunol.* **2011**, *18*, 954–962.
47. Tabrizi, M. A.; Tseng, C. M. L.; Roskos, L. K. Elimination Mechanisms of Therapeutic Monoclonal Antibodies. *Drug Discovery Today* **2006**, *11*, 81–88.
48. Garber, E.; Demarest, S. J.; Broad, A Range of Fab Stabilities within a Host of Therapeutic IgGs. *Biochem. Biophys. Res. Commun.* **2007**, *355*, 751–757.

49. Kumar, V.; Sharma, V. K.; Kalonia, D. S. *In Situ* Precipitation and Vacuum Drying of Interferon Alpha-2a: Development of a Single-Step Process for Obtaining Dry, Stable Protein Formulation. *Int. J. Pharm.* **2009**, *366*, 88–98.
50. Chari, R.; Jerath, K.; Badkar, A. V.; Kalonia, D. S. Long- and Short-Range Electrostatic Interactions Affect the Rheology of Highly Concentrated Antibody Solutions. *Pharm. Res.* **2009**, *26*, 2607–2618.
51. Wallace, B. A.; Janes, R. W. Modern Techniques for Circular Dichroism and Synchrotron Radiation Circular Dichroism Spectroscopy. In *Advances in Biomedical Spectroscopy*; IOS Press: Amsterdam, 2009; p 231.
52. Crowther, J. R. ELISA: Theory and Practice. In *Methods in Molecular Biology*; Humana: Totowa, NJ, 1995; p 223.
53. Arfken, G. B.; Weber, H. J. *Mathematical Methods for Physicists*, 4th ed.; Academic Press: San Diego, CA, 1995; p 1029.
54. Harn, N.; Spitznagel, T.; Perkins, M.; Allan, C.; Shire, S.; Middaugh, C. R. Biophysical Signatures of Monoclonal Antibodies. In *Current Trends in Monoclonal Antibody Development and Manufacturing*; Shire, S. J., Ed.; Springer: New York, 2010; pp 229−246.
55. Hiemenz, P. C.; Rajagopalan, R. *Principles of Colloid and Surface Chemistry*, 3rd ed.; Marcel Dekker, Inc.: New York, 1997; p 650.
56. Miller, M. A.; Engstrom, J. D.; Ludher, B. S.; Johnston, K. P. Low Viscosity Highly Concentrated Injectable Nonaqueous Suspensions of Lysozyme Microparticles. *Langmuir* **2010**, *26*, 1067–1074.
57. Torquato, S.; Truskett, T. M.; Debenedetti, P. G. Is Random Close Packing of Spheres Well Defined? *Phys. Rev. Lett.* **2000**, *84*, 2064–2067.
58. Chakrabarti, R.; Delannoy, J.-Y.; Couty, M.; Schweizer, K. S. Packing Correlations, Collective Scattering and Compressibility of Fractal-like Aggregates in Polymer Nanocomposites and Suspensions. *Soft Matter* **2011**, *7*, 5397–5407.
59. Roosen-Runge, F.; Hennig, M.; Zhang, F.; Jacobs, R. M. J.; Sztucki, M.; Schober, H.; Seydel, T.; Schreiber, F. Protein Self-Diffusion in Crowded Solutions. *Proc. Natl. Acad. Sci. U. S.A.* **2011**, *108*, 11815–11820.
60. Yadav, S.; Liu, J.; Shire, S. J.; Kalonia, D. S. Specific Interactions in High Concentration Antibody Solutions Resulting in High Viscosity. *J. Pharm. Sci.* **2010**, *99*, 1152–1168.
61. Pilz, I.; Puchwein, G.; Kratky, O.; Herbst, M.; Haager, O.; Gall, W. E.; Edelman, G. M. Small Angle X-ray Scattering of a Homogeneous γG1 Immunoglobin. *Biochemistry* **1970**, *9*, 211–219.
62. Miller, D. P.; dePablo, J. J.; Corti, H. Thermophysical Properties of Trehalose and Its Concentrated Aqueous Solutions. *Pharm. Res.* **1997**, *14*, 578–590.
63. Liu, J.; Nguyen, M. D. H.; Andya, J. D.; Shire, S. J. Reversible Self-Association Increases the Viscosity of a Concentrated Monoclonal Antibody in Aqueous Solution. *J. Pharm. Sci.* **2005**, *94*, 1928–1940.
64. Uchida, T.; Nagayama, M.; Gohara, K. Trehalose Solution Viscosity at Low Temperatures Measured by Dynamic Light Scattering Method: Trehalose Depresses Molecular Transportation for Ice Crystal Growth. *J. Cryst. Growth* **2009**, *311*, 4747–4752.